Available online at www.sciencedirect.com
SCIENCE DIRECT®
Journal of Colloid and Interface Science 269 (2004) 164–170
JOURNAL OF Colloid and Interface Science
www.elsevier.com/locate/jcis

Probing with a laser sheet the contact angle distribution along a contact line

E. Rio,[a,b] A. Daerr,[a,b] and L. Limat [a,b,*]

[a] *Laboratoire de Physique et Mécanique des Milieux Hétérogènes, UMR 7636 du CNRS, 10 rue Vauquelin, 75 005 Paris, France*
[b] *Fédération de recherche Matière et Systèmes Complexes, FR CNRS 2438, France*

Received 21 March 2003; accepted 23 July 2003

Abstract

An optical method for probing contact angle distribution along contact lines of any shape using a laser sheet is proposed. This method is applied to a dry patch formed inside a film flowing along an inclined plane, both liquid and solid being transparent. Falling normally to the plane, a laser sheet cuts the contact line and is moved along this line. Distortions of the sheet trace observed on a screen put below the plane allow us to extract the contact angle distribution and the local line inclination along the line. Our results show that the contact angle around a dry patch is nearly constant and equal to the static advancing angle, at least when the evolution of its shape is followed for increasing flow rates. This supports a model of dry patch shape recently proposed by Podgorski and co-workers. Preliminary results obtained for decreasing flow are also qualitatively observed.

Keywords: Wetting; Dewetting; Film flows; Contact angle; Laser sheet

1. Introduction

1.1. General ideas

Contact angle measurements provide a simple method for characterizing the interfacial properties of a solid. Very often, these measurements are performed by direct observations of drops deposited on the solid [1], and viewed from the side. Measurements of the wet area viewed from above can also be used. Better accuracy can be achieved by interferometry (liquid wedge fringes), but this method only holds with small contact angles. Another accurate method proposed by Allain et al. [2] consists in illuminating the drop at normal incidence to the solid with a large laser beam. The beam is reflected by the drop into a light cone, whose angle is a function of the mean contact angle around the drop perimeter.

Contact angle measurements are also important when one wants to model complicated film flows involving contact lines. One can think, for instance, of the now well-known fingering instability that occurs when a liquid begins to flow down a slope [3,4] or of dewetting problems [5,6]. Several methods were used in this context to extract contact angles from experiments and more generally to probe interface shape: light absorption [7], fluorescence [8], and methods based on refraction of light. The simplest idea consists in looking at deformation of a grid across the liquid [9], a method that can be made more accurate with moiré techniques [10]. In another method applied by Buguin et al. [11] to axisymmetric dewetting, a laser beam is deflected by the interface and its deviation is followed versus time while the liquid dewets.

Here we will focus on another contact line problem suggested in Fig. 1: a dry patch left inside a thin film. This problem is related to fingering and dewetting but involves stationary contact lines. These patches are observed in situations of partial wetting, when the flow rate is selected below a critical value [12–15]. Modeling their shape and stability is a difficult free surface hydrodynamical problem, which requires knowledge of how the contact angle is distributed along the contact line surrounding the patch [13,16–19]. Side views are impossible, contact angles are often large, which prevents the use of interferometry [20]; the size of the patch is centimetric and there is no circular symmetry, which prevents using Buguin as well as Allain techniques. In the present paper we describe an optical method similar

* Corresponding author.
E-mail address: limat@pmmh.espci.fr (L. Limat).

0021-9797/$ – see front matter
doi:10.1016/j.jcis.2003.07.005

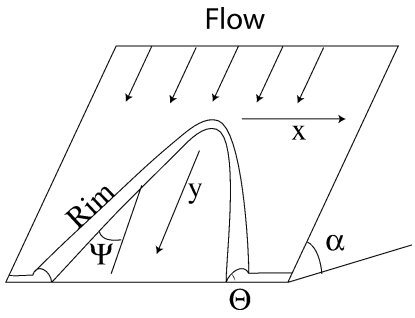

Fig. 1. Sketch of a dry patch left in a film flowing along an inclined plane. A rim around the "dry arch" is collecting the missing liquid.

to that of Allain et al. or to that of Buguin et al. but that uses a laser sheet. It allows localized measurements and allows us to extract contact angle distribution and line inclination in a very simple and visual way. The laser sheet cuts the contact line and is distorted by refraction across the thin liquid prism formed by the liquid wedge very near the line. As we shall see, the "refraction figure" observed on a screen put at finite distance gives directly both the contact angle and the local contact line inclination. This method allows us to build curves giving the contact angle as a function of the position or as a function of the local contact line inclination (angle ψ of Fig. 1), which can be used as a parameter. This method of course implies moving the sheet along the contact line, i.e., in some sense to "scan" it, which is rather easy for a static line but can be a bit more tricky for a moving contact line. However, for a contact line moving in a stationary way (dry patch convected by the flow, drop sliding along an inclined plane, etc.), it is certainly possible to use a static sheet and to follow the sheet trace evolution as a function of time. The setup described here requires that liquid and solid be transparent, but a similar method using reflection instead of refraction is conceivable.

1.2. Dry patch problem

To illustrate our method, we here apply it to the dry patch problem. Owing to their great importance for technical applications (heat exchangers, distillation or cooling devices, desalination plants, nuclear cooling systems, etc.), the shape and stability of dry patches have motivated several papers [13,16–19]. Among these ones, recently, Podgorski et al. carried the first well controlled experimental studies of these patches, on silicon oil films flowing along glass plates coated with low surface energy compounds. Depending on the history of the flow, the situation can be more or less complicated, but they showed that a universal dry patch shape appeared when this shape was recorded for progressively increasing flow rates. They also proposed a simple model of this shape based upon the two following ideas: (1) for progressively increasing flow rates, the contact angle is everywhere very close to the static advancing angle $\theta \simeq \theta_a$, and (2) the shape of the dry patch is mainly governed by a condition of mechanical equilibrium of the rim,

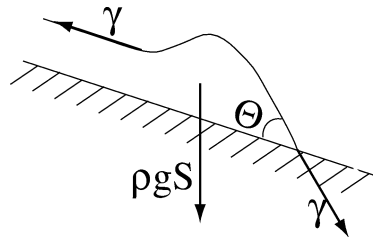

Fig. 2. Mechanical equilibrium of the rim suggested at the dry patch apex.

suggested in Fig. 2 near the dry patch apex. With the notations of Figs. 1 and 2, this balance between capillary effects and the rim weight reads

$$\gamma(1-\cos\theta) = \rho g S(\psi)\sin\alpha\sin\psi, \tag{1}$$

where S designates the cross section of the rim, g stands for gravity, ρ is the liquid mass density, and γ is the surface tension. The angles α and ψ are respectively the plate and contact line inclinations defined in Fig. 1, while θ is the contact angle, assumed to be uniform along the contact line. Still in Podgorski's approach, this equation was to be combined with mass conservation condition $SU = \Gamma x$, where Γ is the flow rate per unit length supplied to the film in its upward region, and U is the mean fluid velocity across the rim cross section. This velocity, driven by the component of gravity parallel to the contact line was approximated by a Poiseuille-type law, the perimeter of the rim cross section being in turn assumed to remain circular. With all these hypotheses, the contact line shape is finally given [17] by the equations

$$x = R\frac{\cos\psi}{\sin^2\psi}, \tag{2}$$

$$y = \frac{R}{3}\left(\frac{1-3\cos^2\psi}{\sin^3\psi} - 1\right), \tag{3}$$

where R is the radius of curvature of the contact line at the dry patch apex. In turn R is given by

$$R = m f_2(\Theta)\frac{l_c^2}{\sin\alpha}\frac{U_c}{\Gamma}, \tag{4}$$

$$f_2(\Theta) = \frac{(1-\cos\Theta)^4}{\Theta - \cos\Theta\sin\Theta}, \tag{5}$$

where $l_c \simeq \sqrt{\gamma/(\rho g)}$ is the capillary length and $U_c = \gamma/\eta$ the capillary velocity built upon surface tension γ and fluid viscosity η. The coefficient m is an unknown numerical factor that takes into account the detailed structure of the flow inside the rim. As explained above, despite its simplicity, this model was found to work remarkably well on isolated dry patches studied for progressively increasing flowrates. Among other reasons, this success was attributed by Podgorski et al. to the uniformity of contact angle along the contact line, assumed to remain very close to the static advancing contact angle θ_a. More quantitatively, in a large range of flow rates, measured shapes are perfectly fitted by Eqs. (2)–(5), with $\theta = \theta_a$ and $m \simeq 0.3$.

Obviously, this hypothesis of a constant contact angle close to a static advancing contact angle is reasonable but would require to be directly checked. One could have also imagined a more complex distribution in which the contact angle would vary continuously along the contact line between the static advancing and receding angles, and this is presumably the most general situation for dry patches of more complicated history. Clearly, the development of our simple method for probing contact angle distribution along the contact line is essential for further progress.

In the present paper we describe our method and we apply it to dry patches formed in the same conditions as in Podgorski et al.: silicon oil films flowing along glass plates coated with appropriate compounds (here fluoropolymers), with evolution of the dry patch shape recorded for a progressively increasing flow rate. Under these conditions, we find that the contact angle is nearly constant along the contact line and equal to the static advancing angle. For the first time, the Podgorski et al. model is supported not only by comparing its prediction with the dry patch shape, but also by direct measurements of contact angle distribution. In Section 2, we describe the experiment together with the principle of our method. Our results on dry patches are presented in Section 3 after a short test of the method on sessile drops. We also give a brief account of what happens when dry patches are followed for decreasing flow rate.

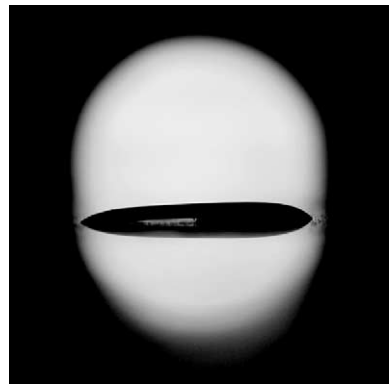

(a)

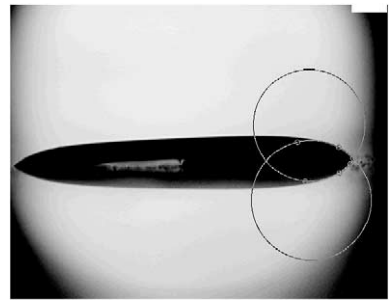

(b)

Fig. 3. (a) Side picture of a centimetric drop about to move on an inclined glass plate (and its reflection in glass). (b) The advancing angle, Θ_a and the receding angle, Θ_r can be extracted from this picture by a construction involving tangent circles.

2. Materials and methods

2.1. How to form regular and isolated dry patches

The hydrodynamic part of our set up is similar to that of Refs. [13,17,18], to which we refer for more details. Its central part is a glass plate of 10 mm thickness and of 40 × 40 cm size, the inclination of which can be turned between $\alpha = 5^\circ$ and $\alpha = 88^\circ$. A part of the upper plate surface is covered with a coating from 3M (fluoropolymers FC 725 diluted with 5/6 of ethyl acetate). This coating allows us to realize partial wetting conditions for the liquid used here, which is a silicon oil (Rhodorsyl 47V20) of surface tension $\gamma = 20.6\,\mathrm{mN/m}$, density $\rho = 0.95\,\mathrm{g/cm^3}$, and viscosity $\eta =$ 21 cP. The relevant static contact angles can be estimated from drops sliding along the plate, in the limit of a vanishing velocity, pictures being taken from the side with a digital camera (5 million pixels) (see Fig. 3). For the experiments presented here this method gives a static advancing angle, $\theta_a = 48^\circ \pm 1^\circ$, and a static receding angle, $\theta_r = 37^\circ \pm 1^\circ$.

At the beginning of the experiment, silicon oil is supplied at constant rate uniformly along the upper edge of the plate through a long thin slot of thickness $H = 0.2$ mm and length $L = 35$ cm. The flowrate is first selected to be high enough ($\Gamma = 2\ \mathrm{cm^3/s}$) to get a uniform flowing film covering the whole plate. After waiting for the disappearance of any transient dry regions left by the initial fingering instability, the flow rate is reduced at a lower value for which the film is only metastable in the central region coated with fluoropolymers (usually a rectangular domain of typical size 10 × 20 cm). Somewhere in this region, film breaking is forced by applying an air jet impulse normally to the free surface during a short time. A dry spot appears and grows until a new equilibrium is reached with a specific shape of the dry patch. The flow rate is then progressively increased step by step to force quasistatic advancing motions of the contact line everywhere, which is assumed to favor a contact angle close to its static advancing value. A typical example of the obtained shape is reproduced in Fig. 4.

These pictures are recorded by a video camera (CCD with a lens of 16 mm) directed normal to the glass plate at a distance of 50 cm. The evolution of this dry patch increasing step by step the flowrate has been recorded. As in Podgorski et al. [13,17,18], this shape is perfectly fitted by Eqs. (2) and (3). For each value of the flowrate, the radius of curvature at the apex of the arch is extracted from the fit. According to Eq. (4), R is expected to be proportional to $l_c^2 U_c/(\Gamma \sin\alpha)$ with a coefficient $m f_2(\Theta)$. Figure 5 shows the evolution of this radius of curvature (R) with the inverse of the flowrate ($1/\Gamma$). When Γ begins to increase, R is constant until the arch begins to close. It seems that the shape of the arch is the same unless Γ is large enough. Our hypothesis is that during this flow increase the contact angle along the contact line grows until being equal to the advancing contact angle. Then the contact line move by quasistatic step and, as

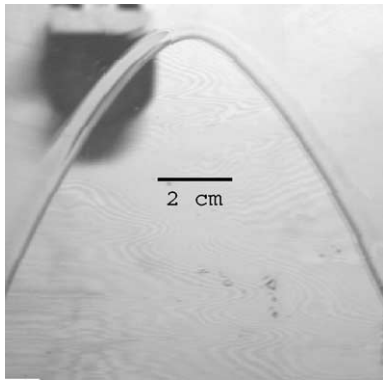

(a)

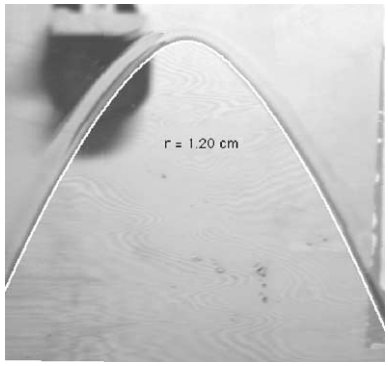

(b)

Fig. 4. (a) Typical picture of a dry arch (silicon oil V20, $\alpha = 50°$, $\Gamma = 0.92$ ml/s). (b) White line: superimposed fit of its shape by Eqs. (2) and (3).

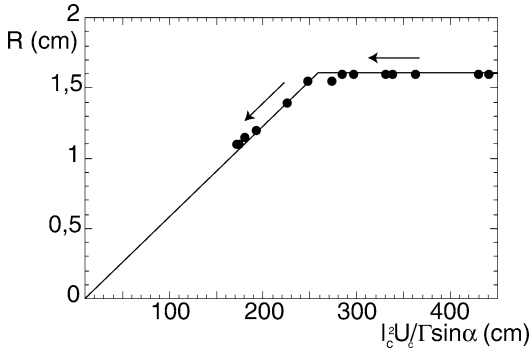

Fig. 5. Evolution of the radius of curvature at the apex increasing the flowrate step by step (silicon oil V20, $\alpha = 50°$), i.e., decreasing $1/\Gamma$ as indicated by the arrows.

expected, R decreases proportionally to $l_c^2 U_c/(\Gamma \sin\alpha)$. The results are in good agreement with Eqs. (2)–(5) with here a coefficient $m = 0.2 \pm 0.05$. In what follows measurements of the contact angle distribution will be mainly performed in the range of linearity of R with respect to $1/\Gamma$.

2.2. Scanning contact angle distribution with a laser sheet

Our method to probe the contact angle distribution around the dry patch is suggested in Fig. 6. A laser sheet is directed normally to the glass plate and intersects this one along a horizontal line that cuts the contact line at two symmetrical

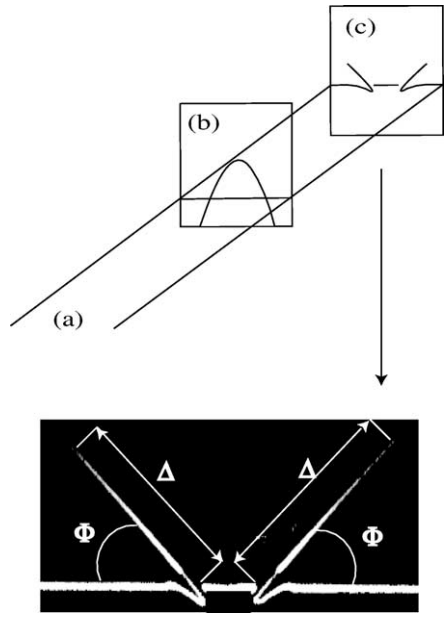

Fig. 6. In our experiment, a laser sheet (a) is refracted by the dry arch (b), the result being visualized on a screen (c) put behind the glass plate.

points. In practice, we have formed this sheet with a laser diode (Lasiris Diode Laser SNF, $\lambda = 637.3$ nm) completed by an appropriate optical head (Lasiris SLH-501). This optical head turns the laser beam into a fan of opening angle 30°, the thickness of which is 200 μm. The diode and its head are placed at a distance of order 50 cm above the glass plate. With an appropriate guiding mechanism, the diode can be moved along the y direction of Fig. 1, in order to explore the whole contact line.

As suggested still in Fig. 6, the sheet is distorted by refraction across the liquid film. These distortions are visualized on a screen (labeled "c" on the figure) put behind the glass plate at a distance of order 15 cm. Roughly, one can distinguish two parts on the obtained "refraction figure." Unperturbed horizontal segments correspond to light rays crossing the dry substrate or the part of the film of uniform thickness. While one excepts a slight shift of their position along y, these rays are not deflected, the light horizontal segments being just the trace of the unperturbed part of the sheet. On the other hand, light rays crossing the rim, especially those in the vicinity of the contact line, are strongly deviated, which results in the appearance of two "light horns" on the refraction figure. These "horns" are characterized by their inclination to the horizontal (labeled Φ on the figure) and their length Δ.

These two quantities, Φ and Δ, contain information on what happens very near to the contact line, because, obviously, the tip of the horns correspond to the most inclined part of the free surface, i.e., in the vicinity of the contact line. Physically, the wedge formed by the liquid near the contact line behaves as a prism that inclines the light rays in a direction normal to contact line and by an amount dictated by its angle, i.e., by the contact angle. This implies a first rela-

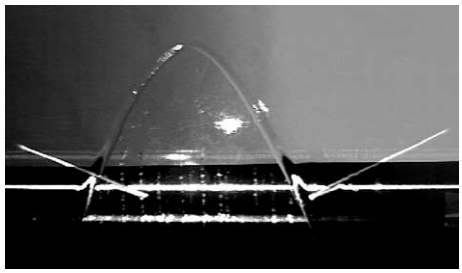

Fig. 7. Laser refraction on the dry arch: view of the dry patch superimposed to a view of the refraction figure, both being taken from the same place. Note that the contact line and the "horn" refracted by this one are perpendicular. To be more clear, the camera has been shift to the right which allow to see both horns and the dry patch.

tionship linking the "horn" inclination to that of the contact line,

$$\Phi = \Psi, \tag{6}$$

i.e., the "horn" and the contact line are perpendicular. This can be seen in Fig. 7, where we have superposed a picture of the arch on a picture of the screen taken by the same video camera, observing both objects from a point situated 50 cm above the glass plate.

Now, the contact angle Θ can be extracted from the "horn" length Δ by applying standard geometrical optics, the paths of light rays in a plane normal to contact line being sketched in Fig. 8. For small angles, the deviation is proportional to the prism angle, i.e., to the contact angle. One gets for small x

$$D = (n-1)\Theta, \tag{7}$$

$$\Delta = (n-1)\Theta\left(d + \frac{e}{n'}\right), \tag{8}$$

where $n = 1.4$ and $n' = 1.4$ are respectively the optical indices of oil and glass, $e \simeq 1$ cm is the glass thickness, and $d \simeq 15$ cm is the distance between the glass plate and the screen. For large angles, the calculation gives a more general set of equations:

$$\Delta = \delta + \delta' = d\tan D + e\tan r', \tag{9}$$

$$\sin D = n\sin(\theta - r), \tag{10}$$

$$n'\sin r' = \sin D, \tag{11}$$

$$n\sin r = \sin\Theta. \tag{12}$$

Moving the laser sheet along from the bottom to the top of the plate, and using Eqs. (9)–(12), one can get the contact angle distribution along the contact line edging the patch as a function of the position or—directly—as a function of the contact line inclination ψ. This parameter being precisely that involved in Podgorski's model, this method appears to be especially well adapted for investigations on dry patches in flowing films.

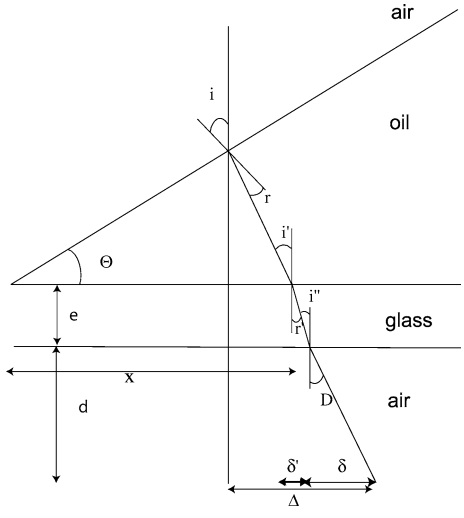

Fig. 8. Refraction of a light ray near contact line.

2.3. Test of the method on sessile drops

To check our optical method, we have compared contact angle measurements obtained on sessile drops with both the laser sheet method and by direct visualizations from the side. For practical reasons linked to the peculiarities of our set up, we found it easier to synthesize solid drops by polymerization of a reticulated silicon (silicon elastomer kit 184 sold by Sylgard) heated at 150° for 1 h. Playing with the history of the drop deposited on diverse substrates (feeding the drop, removing liquid, preliminary heating of its base), we were able to realize several solid drops with different contact angles, which we have deposited on our glass plate in order to probe contact angles at their perimeter. This was not really necessary, but the reticulated silicon has nearly the same optical index as the liquid silicon oil used to form our dry patches ($n = 1.4$), which simplifies the analysis and guarantees that the test of the laser sheet and its application to dry patches are made in the closest possible conditions.

A picture of our solid drops viewed from the side is reproduced in Fig. 9. We have used the same digital camera as in Section 2.1, the picture being taken from the side at a distance from the drop of order 10 cm. The accuracy of the direct determination of contact angle by our tangent circles construction is here of order $\pm 2°$.

The refraction figure (reproduced in Fig. 10) is obtained for the same drop, taking care to treat exactly the same region of its perimeter as above. Several region have been

Fig. 9. Picture of a centimetric polymerized silicon drop taken from the side (about 0.5 mm thick).

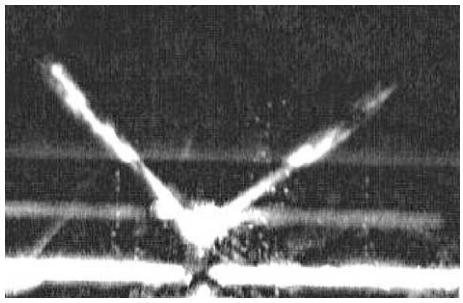

Fig. 10. Refraction figure obtained on the drop of Fig. 9.

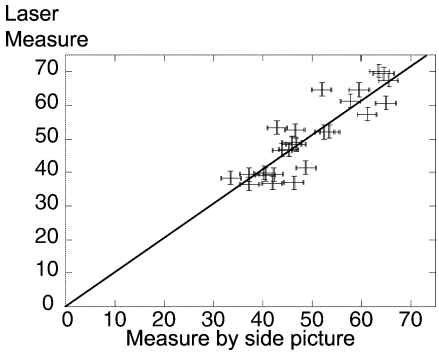

Fig. 11. Comparison between contact angle measured with the laser sheet and with a side picture.

treated on the same drop. Each measurement does not give exactly the same result due to imperfections of drops. Unfortunately, the "horns" are here very thick, which leads to rather poor accuracy, compared to what is possible on dry arches (see the next part). The defects and the smear in the refraction figure are linked to imperfections near the contact line, which possibly arise during the polymerization process, or which are due to small deformation of the solid drop, caused by microscopic differences between its original solidification substrate and the current measurement. We were, however, able to extract a "horn" length and thus a contact angle measured by the laser sheet method, with a rather large error bar. This determination of contact angle is compared to the previous one in Fig. 11. As expected from the error bars, there is a strong scattering of the data, but the linear regression gives a slope nearly equal to 1 (1.02 ± 0.02). This shows that there is no systematic bias in our optical measurement of contact angles.

3. Results and discussion

3.1. Dry patches observed for an increasing flow rate

We have finally applied our laser sheet method to the dry patches described in Section 2. As explained in this section, we took care to work in conditions very similar to those of Podgorski [13]: after nucleation of a dry arch at low flow rate (film rupture induced by blowing), we progressively increased the flow rate. This was made in order to perform

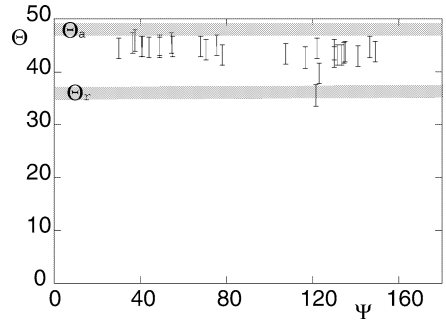

Fig. 12. Measurement of the contact angle along the contact line edging a dry patch observed for increasing flow rate ($\Gamma = 0.64$ ml/s and $\alpha = 60°$).

our contact angle measurements in a range of flow rates, in which the curvature radius of the contact line at the dry patch apex exhibits a linear dependence versus $1/\Gamma \sin(\alpha)$.

The results are given in Fig. 12, for a flowrate equal to $\Gamma = 0.64$ ml/s with $\alpha = 60°$. As appears on this figure, the contact angle is nearly uniform all around the dry patch, and—within the error bars—its value coincide with the static advancing contact angle (here $\theta_a = 48 \pm 1°$). This result is important and means that the hypothesis of a constant contact angle equal to θ_a made by Podgorski et al. was justified. Though this assumption was not the sole involved in their approach, this gives further credence to its relevance at least for dry patches observed for increasing flow rates.

3.2. Dry patches observed for a decreasing flow rate

We have also made some attempts on dry patches observed for a decreasing flow rates. The patch is now progressively opening and the contact line is receding step by step. Before trying the experiment we were qualitatively expecting a radius of curvature following Eq. (4) with a contact angle still uniform but close to the static receding contact angle (here $\Theta_r = 37° \pm 1°$). But experiments show surprising results.

(1) Equations (2) and (3) still fit very well the shape of the arch and the evolution of the radius of curvature is still increasing with $l_c^2 U_c/(\Gamma \sin\alpha)$. But this evolution is irreproducible, the coefficient m depending on the history of the arch. A detailed study of this question is beyond the scope of this paper and will be investigated in a future paper.

(2) The contact angle distribution has been measured while R was increasing (even if it cannot be reproduced) and the result is surprising too. As shown in Fig. 13, the contact angle does not coincide with the static receding contact angle (Θ_r). Moreover, this contact angle cannot be assumed to be uniform along the contact line: the contact angle distribution is more scattered. This scattering is associated to unexpected refraction pictures (see Fig. 14). "Light horns" seem to be cut, doubled, or curved. This is presumably due to the fact that the contact line is pinned on wettability defects. Therefore our laser sheet could also be a promising tool to explore the interface perturbations associated to pinning of contact line on defects. Information about these defects and

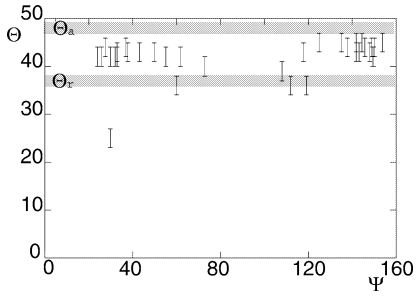

Fig. 13. Contact angle distribution along a receding contact line.

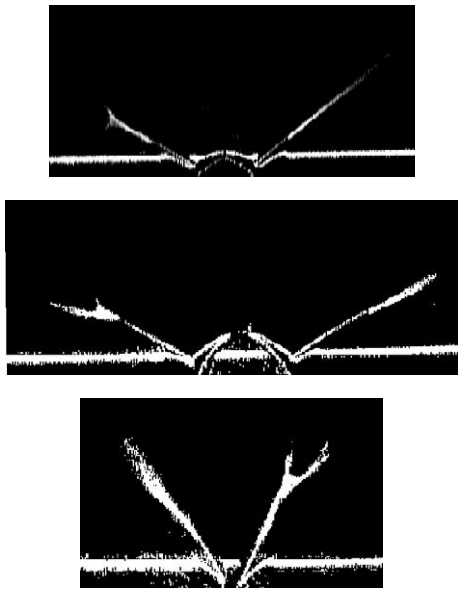

Fig. 14. Surprising refraction pictures due to defects perturbing a receding contact line.

their statistical distribution along the contact line could be extracted from refraction pictures.

4. Conclusion

In summary, the laser sheet allows us to scan the contact angle distribution along a static contact line and the line inclination whatever the complexity of its shape can be. This method uses the refraction of a laser sheet by the liquid wedge formed very near the contact line. We have applied this method to dry patches left inside a film flowing along an inclined plane in situation of partial wetting. When the dry patches are studied for progressively increasing flowrates, we have found a nearly uniform distribution of contact angle all around the patch, the contact angle being nearly equal everywhere to the static advancing angle. This supports the analysis of the patch shape proposed by Podgorski et al. (and also the more complicated one suggested by Wilson [16]), in which this hypothesis played a central role.

The situation seems more complicated when dry patches are observed for a progressively decreasing flow rate. First, and surprisingly, the contact angle remains distinct from the receding angle: it seems that the flow direction has a stronger effect than the direction of motion of the contact line. Next, the contact angle distribution is in general nonuniform and exhibits a strong scattering. This could be associated to the pinning of the contact line on wettability defects, which seems to play a larger role when the contact line recedes than when it advances. The refraction figure seems also here a very promising tool to quantify the action of these defects on the free surface of the liquid very near a contact line.

It would be interesting to generalize this method to nontransparent fluids or solids, for instance, by using reflection of light instead of refraction. Finally, it would also be important to couple refraction figure analysis with high-speed motion of the laser sheet, in order to probe dynamic contact angle distributions on moving contact lines. This could open new issues for various studies raised by coating problems: fingering down a slope [3,4], fingering on spinning disks [21,22], drops sliding down a slope [23], tape or plates withdrawn from a bath [24], air entrainment problems [25].

References

[1] A.W. Adamson, A.P. Gast, Physical Chemistry of Surfaces, Wiley, New York, 1997, Ch. X.
[2] C. Allain, D. Aussere, F. Rondelez, J. Colloid Interface Sci. 107 (1985) 1.
[3] H.E. Huppert, Nature 300 (1982) 427.
[4] N. Silvi, V.F.B. Dussan, Phys. Fluids 28 (1985) 5.
[5] C. Redon, F. Brochart-Wyart, F. Rondelez, Phys. Rev. Lett. 66 (1991) 75.
[6] G. Reiter, Phys. Rev. Lett. 68 (1992) 75.
[7] R.T. Goodwin, An Investigation of a Viscous Coating Flow, Ph.D. thesis, Stanford University, 1991.
[8] M.F.G. Johnson, R.A. Schutler, S.G. Bankoff, Rev. Sci. Instrum. 68 (11) (1997) 4097–4102.
[9] C. Andrieu, C. Sykes, F. Brochart-Wyart, J. Adhesion 58 (1996) 15.
[10] H.S. Khesgi, L.E. Scriven, Chem. Eng. Sci. 38 (1983) 525.
[11] A. Buguin, L. Vovelle, F. Brochart-Wyart, Phys. Rev. Lett. 83 (1999) 1183.
[12] D.E. Hartley, W. Murgatroyd, Int. J. Heat Mass Transfer 7 (1964) 1003.
[13] T. Podgorski, Ruissellement en condition de mouillage parteil, Thèse de doctorat, Université Paris VI, 2000.
[14] A.B. Ponter, A. Davies, T.K. Ross, P.G. Thornley, Int. J. Heat Mass Transfer 10 (1967) 349.
[15] S.G. Bankoff, Int. J. Heat Mass Transfer 14 (1971) 2143.
[16] S.D.R. Wilson, Int. J. Heat Mass Transfer 17 (1974) 1607–1615.
[17] T. Podgorski, J.M. Flesselles, L. Limat, Phys. Fluids 11 (1999) 845.
[18] T. Podgorski, J.-M. Flesselles, L. Limat, C. R. Acad. Sci. Paris Sér. IV 2 (2001) 1361–1367.
[19] S.K. Wilson, B.R. Duffy, S.H. Davis, Eur. J. Appl. Math. 12 (2001) 233.
[20] A.-M. Cazabat, F. Heslot, S.M. Troian, P. Carles, Nature 346 (1990) 824.
[21] F. Melo, J.F. Joanny, S. Fauve, Phys. Rev. Lett. 63 (1989) 1958.
[22] I. Veretnnikov, A. Agarmal, A. Indeikina, H.-C. Chang, J. Colloid Interface Sci. 215 (1999) 425.
[23] T. Podgorski, J.-M. Flesselles, L. Limat, Phys. Rev. Lett. 87 (2001) 036102.
[24] T.D. Blake, J.M. Haynes, Nature 282 (1979) 489.
[25] R. Burley, B.S. Kennedy, Chem. Ing. Sci. 31 (1976) 901.